NUMERICAL STUDY OF THE BOILING PROCESS IN THREE-DIMENSIONAL MICROPORES

Shebelev A. V. [1] , **Zaitsev D. V.** , **Kabov O. A.**

Abstract In this work, a model for direct numerical simulation of the boiling process on three-dimensional porous surfaces is proposed and tested. To solve this problem, the VOF method was applied using the CSF method to simulate surface tension. Images of formation of vapor bubbles and value of the heat transfer coefficient were obtained depending on substrate temperature, pore material, backfill geometry, and contact angle.

Key words: heat transfer, boiling, heat transfer coefficient, porous medium.

AMS Mathematics Subject Classification: 76R10.

1 Introduction

Classic air and water cooling is suitable for heat dissipation in many industries. However, due to the increasing heat flux densities in various devices, it has become necessary to resort to various tricks for the continued use of single-phase cooling systems. Improvements were primarily required for power microelectronics, computational microelectronics, laser systems and other industries. At the same time, optimisation of two-phase cooling leads to a reduction in size and mass of already used devices, such as air conditioner radiators [1] or refrigeration devices [2], which leads to a reduction in their material intensity and cost.

In microelectronics, heat pipes and evaporation chambers are mainly used for heat dissipation. These devices use a porous medium to transfer heat from a high-temperature region to a low-temperature region. The porous medium acts as a wick, transferring fluid from hot part of the heat pipe to cold part due to the capillary effect. The thermal resistance of the porous medium is a significant problem for heat transfer to the evaporator section [3]. The main mechanisms of phase transitions in a heat pipe are evaporation and condensation at the liquid-vapor interface. At a certain heat flux, a bubble boiling regime of liquid is realized in the wick, which leads to a noticeable decrease in thermal resistance. This phenomenon was observed in previous studies [4, 5].

Previous studies have shown that applying a porous coating to the surface of a flat plate increases the heat transfer coefficient for nucleate boiling. However, the porous coating increases the thermal resistance between the heated surface and the vapor. In addition, two factors can significantly affect the increase in heat transfer: an increase

---

[1]Corresponding Author.

in the number of vaporization sites due to the use of a porous surface and an increase in the rate of heat transfer during the phase transition due to an increase in the number and speed of bubble detachment from the surface. To clarify the mechanisms, a deeper understanding of the process of vapor bubble growth in a porous structure is necessary. Numerous studies, such as the one presented in [6], have experimentally studied porous structures during boiling.

The backfill method and its porosity (anisotropic or isotropic) are also of great importance. As shown in [7], anisotropic backfill with a porosity in the range of 50-71% showed the most effective heat transfer results. This is due to the fact that steam bubbles are able to leave the vaporization zone at a higher speed than in the case of lower porosity. The isotropic backfill method leads to lateral growth of steam bubbles, which subsequently form a continuous vapor region. This negatively affects the heat transfer rate. In addition, work [7] considered the optimization of the wick height in a porous medium. The results showed that the optimal height-to-width ratio is 4-5.

The behavior of vapor bubbles is affected by many factors: resistance force, surface tension force, bubble size when breaking away from the surface, pore size, porosity coefficient, and many others. All these parameters must be taken into account when modeling boiling on a porous surface. Therefore, in this paper, a systematic study of the boiling process was carried out for various pore configurations, pore material, material wettability, and heater temperature. To solve this problem, the VOF method with the CSF scheme for modeling surface tension was used, which was verified on the problem of boiling on a flat plate [8].

2   Mathematical model

Today, the most widely used methods are those implementing the idea of markers. Due to its efficiency and ease of implementation, the Volume of Fluid (VOF) method [9] has gained the greatest popularity today, having proven itself well for calculating flows with a free surface. The idea of this method is that liquid and gas are considered as a single two-component medium, and the spatial distribution of phases within the calculation domain is determined using a special marker function F(x, y, z, t). The volume fraction of the liquid phase in the calculation cell is taken to be F(x, y, z, t) = 0 if the cell is empty, F(x, y, z, t) = 1 if cell is completely filled with liquid and 0 < F(x, y, z, t) < 1 if phase boundary passes through the cell.

Since the free surface moves together with the liquid, tracking the movement of the free boundary in space is carried out by solving the equation for the transfer of the volume fraction of the liquid phase in the cell:

$$\frac{\partial F}{\partial t} + \mathbf{v} \cdot \nabla F = 0 \tag{1}$$

where: $\mathbf{v}$ is velocity vector of a two-phase medium, found from the solution of a system of hydrodynamic equations consisting of the equation of conservation of mass or the equation of continuity:

$$\frac{\partial \rho}{\partial t} + \nabla(\rho \mathbf{v}) = 0 \tag{2}$$

and the motion equation:

$$\frac{\partial \rho \mathbf{v}}{\partial t} + \nabla(\rho \mathbf{v} \mathbf{v}) = -\nabla P + \nabla \mathbf{T} + \mathbf{F}_s + \rho \mathbf{g} \tag{3}$$

here: $\mathbf{T}$ is viscous stress tensor, $\mathbf{F}_s$ is volume force vector, P is static pressure and ρ is density of a two-phase liquid. Components of the viscous stress tensor τ_{ij}:

$$\mathbf{T}_{ij} = \mu \left(\frac{\partial u_i}{\partial x_i} + \frac{\partial u_j}{\partial x_j} \right) \tag{4}$$

where: μ is coefficient of dynamic viscosity of a two-phase liquid.

The density and molecular viscosity of the two-component medium under consideration are determined through the volume fraction of the liquid phase in the cell according to the mixing rule:

$$\rho = \rho_l F + (1 - F)\rho_v \tag{5}$$

$$\mu = \mu_l F + (1 - F)\mu_v \tag{6}$$

here: ρ_l, μ_l is density and viscosity of liquid ρ_v, μ_v is density and viscosity of vapor.

To model the surface tension in this problem, the CSF (Continuum Surface Force) algorithm [10] was used, which involves introducing an additional volumetric force $\mathbf{F}_s$ into the equations of motion. The magnitude of this force is determined from the relationship:

$$\mathbf{F}_s = \sigma k \nabla F \tag{7}$$

where: σ is coefficient of surface tension, k is curvature of the free surface, defined as the divergence of the normal vector:

$$k = \nabla\left(\frac{\mathbf{n}}{|n|}\right) \tag{8}$$

The normal to the free surface is calculated as the gradient of the volume fraction of the liquid phase in the cell:

$$\mathbf{n} = \nabla F \tag{9}$$

The magnitude of the normal vector is determined by the contact angle θ on the solid wall:

$$\mathbf{n} = \mathbf{n}_w \cos\theta + \tau_w \sin\theta \tag{10}$$

here k_w, τ_w is normal and tangential components of a vector.

Energy equation:

$$\frac{\partial}{\partial t}(\rho h) + \nabla(\mathbf{v}\rho h) = \nabla(k_{eff}\nabla T) + S_h \tag{11}$$

where enthalpy h is defined as:

$$h = \int_{T_{ref}}^{T} C_p dT \tag{12}$$

The effective thermal conductivity k_{eff} is defined as:

$$k_{eff} = \alpha_l k_l + (1 - \alpha_l) k_v \tag{13}$$

The term S_h in this equation represents the volumetric heat source due to the phase change at the interface:

$$S_h = -\dot{m}_{lv} h_{lv} \tag{14}$$

here: $\dot{m}_{lv}$ is rate of mass transfer from liquid to vapor, $\dot{m}_{vl}$ is rate of mass transfer from vapor to liquid, and h_{lv} is latent heat of vaporization from liquid to vapor.

The rate of mass transfer is realized using the Lee model:

$$\begin{aligned}
\dot{m}_{lv} &= \gamma_l \alpha_l \rho_l \frac{(T_l - T_{sat})}{T_{sat}} \text{if} T_l > T_{sat} \\
\dot{m}_{vl} &= \gamma_v \alpha_v \rho_v \frac{(T_{sat} - T_v)}{T_{sat}} \text{if} T_v < T_{sat}
\end{aligned} \tag{15}$$

where the constant γ has the dimension $1/s$ and is defined as:

$$\gamma = \frac{6}{d_b} \beta \sqrt{\frac{M}{2\pi R T_{sat}}} L \left(\frac{\alpha_v \rho_v}{\rho_l - \rho_v} \right) \tag{16}$$

here: β is accommodation coefficient, d_b is bubble diameter, M is molar mass, R is universal gas constant, T_{Ssat} is boiling point and L is latent heat of vaporization.

After analyzing the works [7, 11, 12], the constant γ in this work was taken equal to 100 for both evaporation and condensation.

3 Three-dimensional formulation of the problem

For the three-dimensional formulation, a geometry was constructed with balls of 150 microns in diameter, which overlap each other by 10 microns, forming an uniformed porous structure, shown in Figure 1a on the left. A geometry with a chess order of balls was also constructed (Figure 1a on the right). The total size of the computational domain is $0.83 * 0.83 mm$ in the XY plane and 1.2 mm in height. Symmetry conditions are set on the side walls ($\upsilon_x = 0 \quad \frac{\partial \mathbf{v}}{\partial x} = 0 \quad \frac{\partial T}{\partial x} = 0 \frac{\partial \alpha_v}{\partial x} = 0$), non-slip conditions are set on the walls ($\mathbf{v} = \mathbf{v}_w$), on the top wall - free outlet($p = 0 \quad \frac{\partial u}{\partial z} = 0 \quad \frac{\partial \alpha_v}{\partial z} = 0$) and ($\alpha_l = 1 \quad T = 370$)for the backflow, a constant temperature is set on the lower wall ($T = const$). The convective terms of the hydrodynamic equations are approximated by the second-order upwind QUICK scheme [13]. The non-stationary terms of the hydrodynamic equations are approximated by the first-order implicit scheme. The energy equation is approximated by the second-order upwind scheme [13]. The VOF equations are solved by the Geo-Reconstruct [13] scheme. The diffusion fluxes and source terms are approximated to the second order. The relationship between the velocity and pressure fields is implemented by the Piso [13] procedure. The porous structure and substrate materials were varied, and a constant temperature was set on the bottom wall of the substrate. The contact angle was chosen to be $120°$. Gravity is directed against the Z axis. A polyhedral grid with a minimum step of 4 microns (Figure 1b) and a total number of cells of 2 million is constructed. At the initial moment of time, the region is filled with water with a temperature of 370K, the temperature of
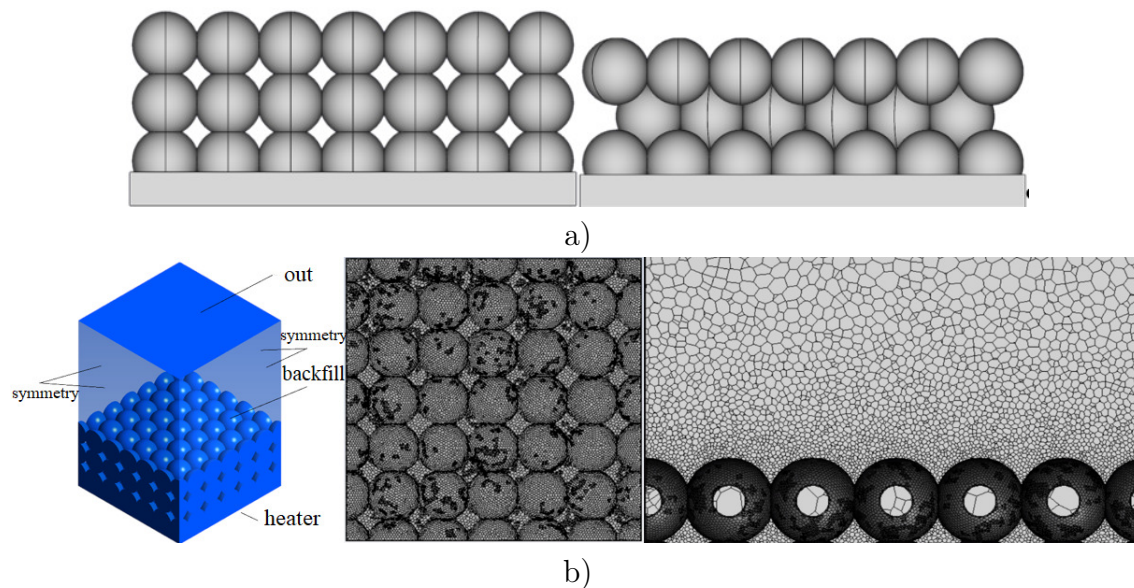
Figure 1: Statement of the problem: a) geometry of the problem, b) boundary conditions and a fragment of the grid on the surface of the porous backfill and in the central section.

the substrate and the porous structure is also 370K. At the exit, there is a condition of return flow with a temperature of 370K.

The thermophysical properties of water and vapor are presented in Table 1, where ρ is density, μ is viscosity, λ is thermal conductivity, C_p is heat capacity, L is latent heat of vaporization, σ is surface tension. For correct resolution of the water-steam interface and numerical stability of the calculation, the Courant number (CFL) was taken equal to one. These calculations were performed in the Ansys Fluent software package [13].

Table 1: Thermophysical properties

	ρ, kg/m^3	μ, Pa s	λ, W/m K	C_p, J/kg K	L, kJ/kg	σ, N/m
Water	958	$2.8 \cdot 10^{-4}$	0.68	4216	-	-
Water vapor	0.597	$1.21 \cdot 10^{-}$	0.025	2034	-	-
Water vapor transition	-	-	-	-	2270	0.058

4   Effect of temperature on the heater

The study of the influence of the heater temperature was carried out in the following formulation: the position of the balls in the backfill is uniform. The material of the porous structure and the substrate is copper, a constant temperature was set on the lower wall of the substrate: 375K, 378K, 383K.

Figures 2-4 show heating process of the calculated volume. In Figure 2, only bottom
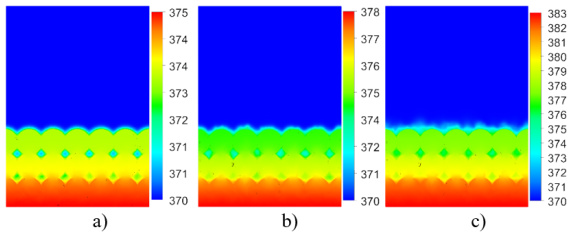
Figure 2: Temperature distribution in the middle section of the porous backfill and substrate at a time of $6 \cdot 10^{-4}$ s for the initial temperature: a) 375K b) 378K c) 383K.
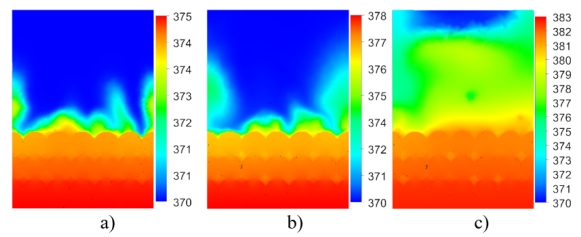
Figure 3: Temperature distribution in the middle section of the porous backfill and substrate at a time of $3.5 \cdot 10^{-3}$ s for the initial temperature: a) 375K b) 378K c) 383K.
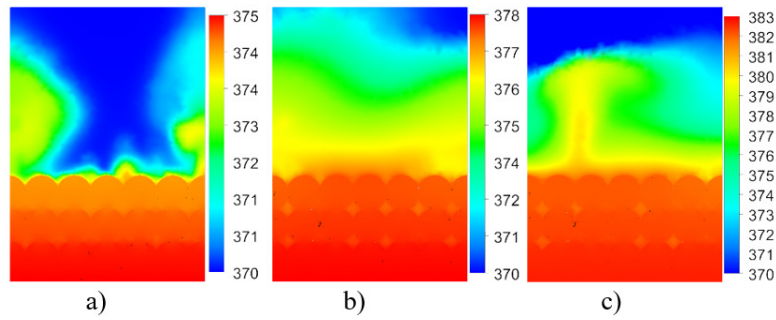
Figure 4: Temperature distribution in the middle section of the porous backfill and substrate at a time of $1 \cdot 10^{-2}$ s for the initial temperature: a) 375K b) 378K c) 383K.
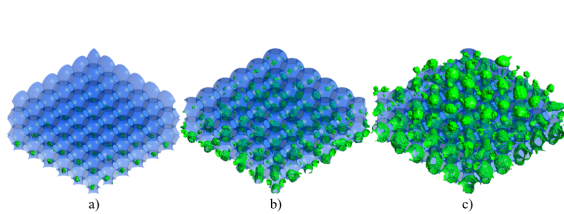
Figure 5: Distribution of the vapor isosurface at a time of $6 \cdot 10^{-4}$ s for the initial temperature: a) 375 K b) 378 K c) 383 K.
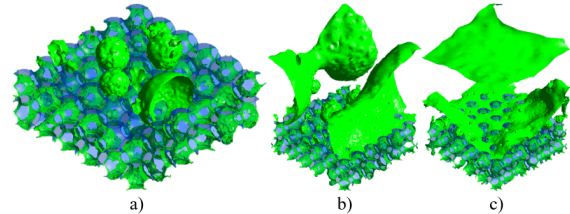
Figure 6: Distribution of the vapor isosurface at a time of $3.5 \cdot 10^{-3}$ s for the initial temperature: a) 375 K b) 378 K c) 383 K.

row of balls has heater temperature for all initial temperatures. In Figure 3, all backfill rows already have heater temperature. Also, Figures 3a and 3b show several small convective streams. Figure 4c show formation of one clear convective stream rising from the balls. Since there is a condition for reverse flow at outlet with a temperature of 370K, there are always areas with a lower temperature at the upper boundary, where partial condensation of steam and its return to the pores occurs.

Fig. 5-6 show the isosurfaces of vapor at different moments in time. In Fig. 5a, small pockets of vapor are formed in the area between the first row and the heater. In Fig. 5b, the vapor phase is already between the first and second row of balls. In Fig. 5c, vapor has formed in all internal pores, passed through them, and a massive detachment of bubbles from surface of third row of backfill occurs. In Fig. 6a, several

bubbles, size of a backfill ball, have formed on surface of backfill. In Fig. 6b, the steam bubbles have merged near the boundary of the computational domain, and there are single bubbles in the center. In Fig. 6c, a continuous film of steam has already formed and almost reached the upper boundary.
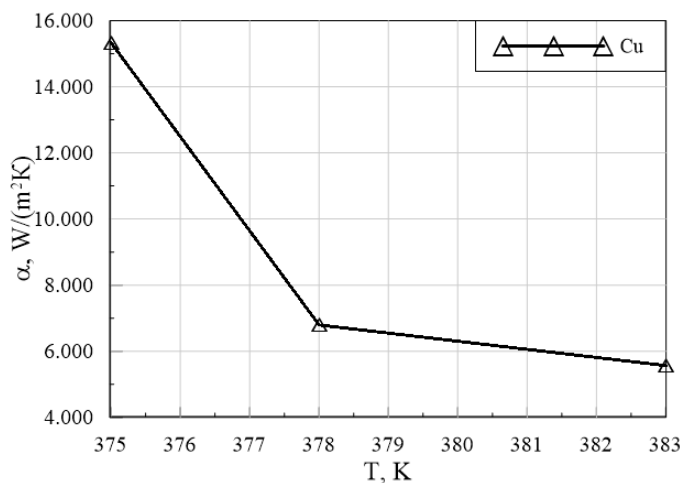
Figure 7: Average heat transfer coefficient on the backfill walls depending on the backfill temperature

Figure 7 shows average heat transfer coefficient on backfill wall depending on backfill temperature. It is evident that with increasing temperature the heat transfer coefficient drops almost 3 times. This is due to the fact that with increasing temperature a continuous film of vapor quickly forms, which prevents effective heat transfer from backfill.

5 Effect of backfill material

The study of the influence of the backfill material was carried out in the following formulation: the position of the balls in the backfill is uniform. The material of the porous structure and the substrate is copper, silicon or iron, a constant temperature of 378K was set on the lower wall of the substrate.

Only at the initial stage of heating (Fig. 8) all materials have the same temperature of all rows of backfill. In Fig. 9 the temperature of the upper rows of balls and the mixture of liquid and vapor above them is higher for copper and silicon.

The process of vapor formation is similar to Fig. 5-6, only slower and less intense, since iron and silicon have greater thermal resistance. However, at a temperature of 378K silicon has the highest heat transfer coefficient, since vapor film above the ball backfill is not as stable as for copper.

Figure 10 shows the average heat transfer coefficient on the backfill wall depending on the backfill temperature. For all materials, a tendency is also visible that with increasing temperature, the heat transfer coefficient drops almost 3 times. At a temperature of 375K, the heat transfer coefficient of silicon is 22% less than that of copper.
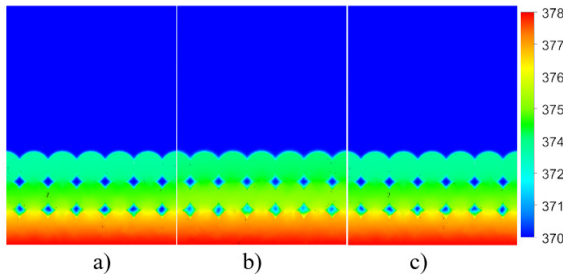
Figure 8: Temperature distribution in the middle section of the porous backfill and substrate for an initial temperature of 378K at a time of $1.5 \cdot 10^{-4}$ s for materials: a) copper b) silicon c) iron.
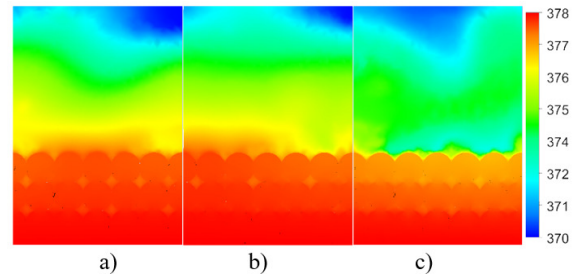
Figure 9: Temperature distribution in the middle section of the porous backfill and substrate for an initial temperature of 378K at a time of $1 \cdot 10^{-2}$ s for materials: a) copper b) silicon c) iron.
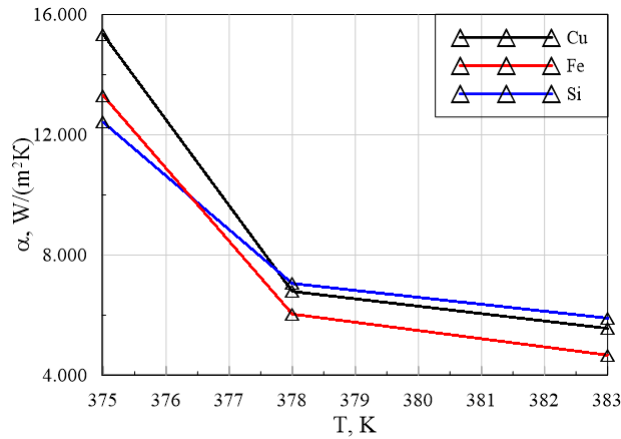
Figure 10: Average heat transfer coefficient on the backfill walls depending on the backfill temperature

At a temperature of 378K and 383K, vise verse, the heat transfer coefficient of silicon is slightly greater than that of copper, and that of iron is 29% less, which is associated with the lowest thermal conductivity coefficient.

6 Effect of backfill geometry

The study of the influence of the backfill geometry was carried out in the following formulation: the position of balls in backfill is uniform or chess order. The material of the porous structure and the substrate is copper, on the lower wall of which a constant temperature was set: 375K, 378K, 383K.

Figure 12 shows that with a chess backfill, heating of all rows occurs faster, which is associated with an increased contact area between the rows.

In figures 13(b) and 14(b) it is evident that for chess backfill, due to fact that heating is more intense, the process of vapor formation is also faster. Thus, by the time of $6 \cdot 10^{-4}$ s, vapor bubbles come out of all pores, whereas for the uniform backfill, bubbles are formed only between the first and second rows of the backfill. However,
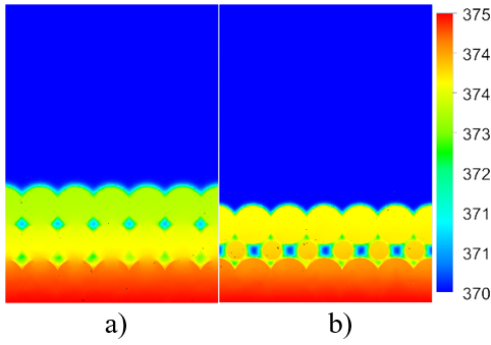
Figure 11: Temperature distribution in the average cross-section of the porous backfill and substrate at a time of $6 \cdot 10^{-4}$ s for a temperature of 375 K and different backfill: a) uniform b) chess order.
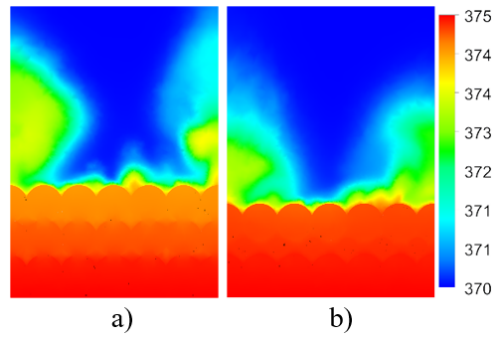
Figure 12: Temperature distribution in the average cross-section of the porous backfill and substrate at a time of $1 \cdot 10^{-2}$ s for a temperature of 375 K and different backfill: a) uniform b) chess order.
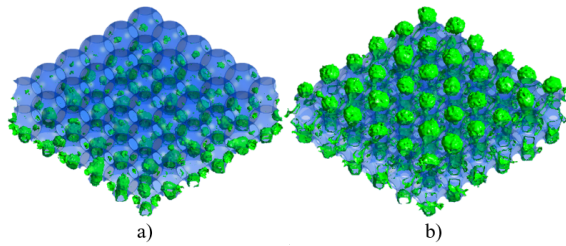
Figure 13: Distribution of the vapor iso-surface at time $6 \cdot 10^{-4}$ s for different back-fill: a) uniform b) chess order.
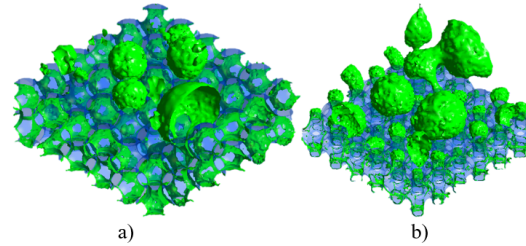
Figure 14: Distribution of the vapor iso-surface at time $3.5 10^{-3}$ s for different back-fill: a) uniform b) chess order.

further intensive movement of vapor in pores for chess backfill does not occur, for reason that the shape of the internal channels is complex, and their size is smaller than for uniform backfill.
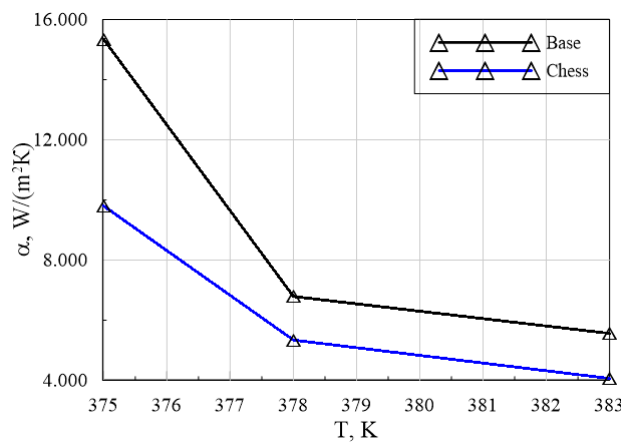
Figure 15: Average heat transfer coefficient on the backfill walls depending on the backfill temperature.

Fig. 15 show heat transfer coefficient for chess backfill is less from 20% to 35% than for an uniform one. This is due to the too rapid evaporation of water inside
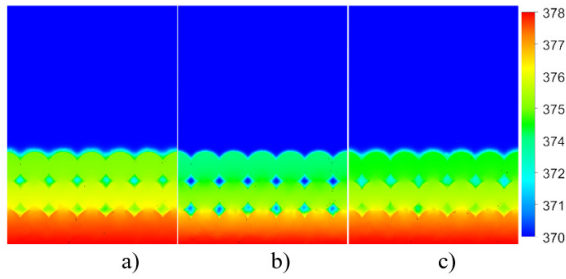
Figure 16: Temperature distribution in the middle section of the porous backfill and substrate for an initial temperature of 378K at a time of $6 \cdot 10^{-4}$ s for different contact angles: a) 64° b) 120° c) 150°.
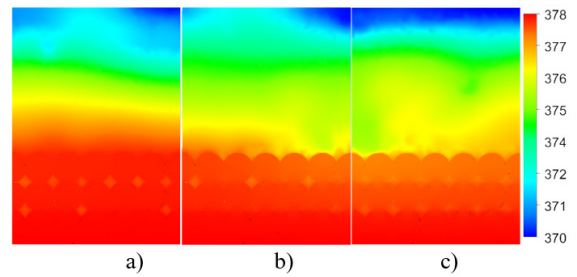
Figure 17: Temperature distribution in the middle section of the porous backfill and substrate for an initial temperature of 378K at a time of $1 \cdot 10^{-2}$ s for different contact angles: a) 64° b) 120° c) 150°.

the pores and the lack of external water inflow, since the pore channels are occupied by vapor, as well as the smaller effective area of the backfill compared to a uniform backfill.

7 Effect of contact angle

The study of the influence of the contact angle of wetting was carried out in the following formulation: the position the balls in the filling is uniform, material of the porous structure and the substrate is silicon. A constant temperature of 378 K was set on the lower wall of the substrate. The contact angle of wetting varied from 64° to 150°.

Figure 16 shows the temperature distribution in middle section of backfill. Faster heating of rows occurs at a wetting angle of 64°. Figure 17 also shows that at a wetting angle of 64°, a flat horizontal temperature profile is formed and there is no vertical mixing. It is also seen that at a wetting angle of 120° and 150°, the temperature of different backfill rows differs (Figure 17b and Figure 17c), in contrast to a wetting angle of 64°, since there is no blocking of the hot surface by the film of the formed steam.
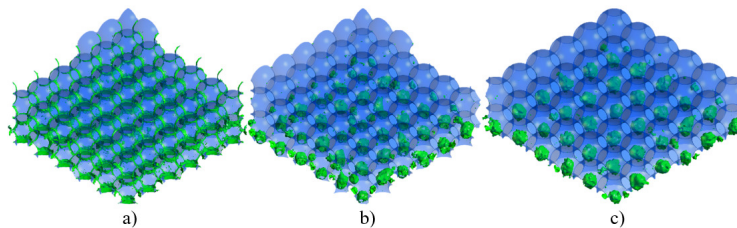
Figure 18: Distribution of the vapor isosurface at a time of $6 \cdot 10^{-4}$ s for different contact angles: a) 64° b) 120° c) 150°.

At the initial stage of heating (Fig. 18a), a film of vapor is formed at the junction of the surfaces of balls, and not in pores, as in Fig. 18b and Fig. 18c. The resulting vapor film on the surface of the balls partially blocks the transfer of heat from the solid
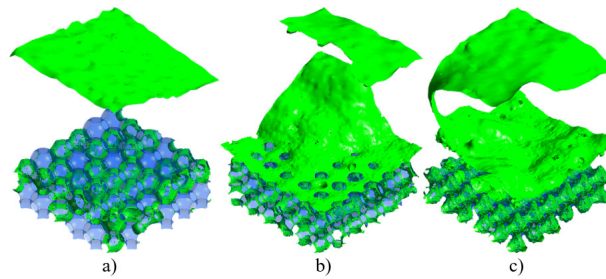
Figure 19: Distribution of the vapor isosurface at a time of $1 \cdot 10^{-2}$ s for different contact angles: a) 64° b) 120° c) 150°.

to the liquid (Fig. 19a). A continuous, smooth region of vapor is also formed above the surface of the fill, which increases due to boiling inside the pores (Fig. 19a). For a contact angle of 120° and 150°, the mechanism of the boiling process is different: bubbles are quickly removed from the pores, joining on the surface of the fill, forming an uneven film in which vertical mixing occurs and reaching the upper boundary, where the vapor condenses, flows back into the area above the fill.
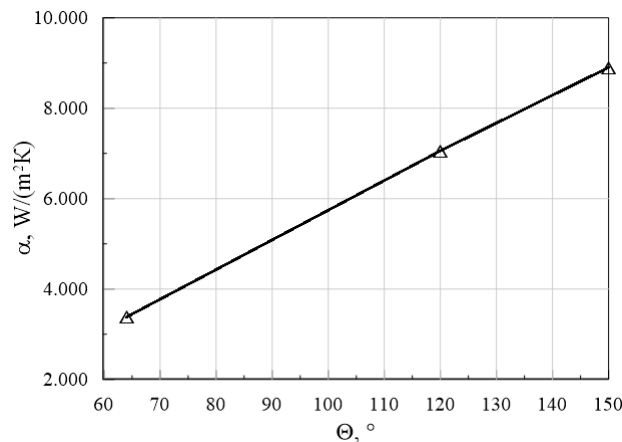
Figure 20: Average heat transfer coefficient on the backfill walls depending on the contact angle.

Fig. 20 shows that the heat transfer coefficient increases linearly with increasing contact angle, from a hydrophilic surface to a hydrophobic one. The increase is 2.3 times with a change in contact angle from 64° to 150°. This is due to the intensification of vapor movement from the pores for large contact angles.

Conclusion

Systematic studies of the characteristics of heat and mass transfer during boiling in the volume and on the surface of a capillary-porous coating were carried out.

The effect of temperature on a porous body was studied. Temperature distribution patterns were obtained, as well as bubble formation. It was shown that with an increase in temperature, the heat transfer coefficient drops almost 3 times. This is due to the fact that with an increase in temperature, a continuous film of steam quickly forms, which prevents effective heat transfer from the backfill.

The effect of porosity and permeability of the coating on heat and mass transfer during boiling was systematically studied. Temperature distribution patterns were obtained, as well as bubble formation. With a chess filling, the bubble formation process occurs faster at the initial stage, but due to the more complex shape of the channels, the bubbles leave the inner area more slowly and the effective surface area is 13% smaller, the heat transfer coefficient is 20-35% lower depending on the temperature of the porous coating than for an uniform structure.

The influence of thermal resistance of the coating material was studied. At a temperature of 375K, the heat transfer coefficient of silicon is 22% less than that of copper. At a temperature of 378K and 383K and vise verse, the heat transfer coefficient of silicon is slightly greater (10%) than that of copper, and that of iron is 29% less, which is associated with the lowest thermal conductivity coefficient.

The influence of the wettability of the porous coating material on the boiling characteristics of the liquid inside and on the coating surface was studied. The increase is 2.3 times for silicon when the wetting angle changes from 64° to 150°. This is due to the intensification of the movement of steam from the pores for large wetting angles.

Acknowledgement

References

[1] Wang S.H., Rose J.W., *Theory of heat transfer during condensation in microchannels*, Int. J. Heat Mass Transf, Vol.54 (2011).

[2] Munkejord S.T., Mhlum H.S, Zakeri G.R., Neksa P., *Micro technology in heat pumping systems*, Int. J. Refrig, Vol 25 (2002), 471-478.

[3] Weibel J.A., Garimella S.V., North M.T., *Characterization of evaporation and boiling from sintered powder wicks fed by capillary action* , International Journal of Heat and Mass Transfer, Vol. 53 (2010).

[4] Altman D.H., Wasniewski J.R., North M.T., Kim S.S., Fisher T.S., *RDevelopment of Micro/Nano Engineered Wick-Based Passive Heat Spreaders for Thermal Management of High Power Electronic*, Devices Proceedings of the ASME InterPACK Portland,(2011).

[5] Chien L.H., Chang C.C., *Experimental Study of Evaporation Resistance on Porous Surfaces in Flat Heat Pipes*, Thermomechanical Phenomena in Electrical Systems вЋ" Proceedings of the Intersociety Conference, (2002).

[6] Ranjan R., Murthy J.Y., Garimella S.V., *Bubble dynamics during capillary-fed nucleate boiling in porous media*,13th IEEE ITHERM Conference, Vol. 12 (2012).

[7] Lee J., O′Neill L.E., Mudawar I., *3-D computational investigation and experimental validation of effect of shear-lift on two-phase flow and heat transfer characteristics of highly subcooled flow boiling in vertical upflow* ,International Journal of Heat and Mass Transfer, Vol. 150 (2020).

[8] Shebelev A., Lobasov A., Zaitsev D., Kabov O., *Numerical investigation of boiling process in micropores* ,E3S Web of Conferences, Vol. 459 (2023).

[9] Hirt C.V., Nichols B.D., *Volume of fluid (VOF) method for the dynamics of free boundaries*,Journal of computational physics, Vol. 39 (1981) 201-226.

[10] Brackbill J.U., Kothe D.B., Zemach C.A., *Continuum method for modeling surface tension* ,J. Comput. Phys., Vol. 100 (1992) 335-354.

[11] Lee H., Kharangate C.R., Mascarenhas N., Park I., Mudawar I., *Experimental and computational investigation of vertical downflow condensation* ,International Journal of Heat and Mass Transfer, Vol. 55 (2015).

[12] Devahdhanush V.S., Lei Y., Chen Z., Mudawar I., *Assessing advantages and disadvantages of macro- and micro-channel flow boiling for high-heat-flux thermal management using computational and theoretical/empirical methods*,International Journal of Heat and Mass Transfer, Vol. 169 (2021).

[13] *Ansys Fluent Documetation*

Shebelev A.V.,
Kutateladze Institute of Thermophysics SB RAS
Lavrentieva пïSv., 1, 630090 Novosibirsk, Russia
Siberian Federal University,
Svobodnyi av., 79, 660041 Krasnoyarsk, Russia,
Email: `aleksandr-shebelev@mail.ru`,

Kabov O.A.,
Kutateladze Institute of Thermophysics SB RAS
Lavrentieva av., 1, 630090 Novosibirsk, Russia
Email: `kabov@itp.nsc.ru`.

Zaitsev D.V.,
Kutateladze Institute of Thermophysics SB RAS
Lavrentieva пïSv., 1, 630090 Novosibirsk, Russia
Email: `zaitsev@itp.nsc.ru`,